Plasmonics (2022) 17:1361–1368
https://doi.org/10.1007/s11468-022-01602-1

Switchable Gratings for Ultracompact and Ultrahigh Modulation Depth Plasmonic Switches

Sandeep Kumar Chamoli[1,2] · Mohamed ElKabbash[3] · Chunlei Guo[3]

Received: 15 July 2021 / Accepted: 18 January 2022 / Published online: 10 May 2022

Abstract

Plasmonic interconnects present a compact platform for high modulation-depth optical switches. Conventional plasmonic switching approaches depend on modifying the dispersion of the surface plasmon polariton (SPP) wave at the metal/dielectric interface. Here, we introduce a novel scheme for ultracompact and high modulation depth (MD) plasmonic switching using a phase-change material-based switchable grating consisting of antimony trisulfide (Sb_2S_3). In its ON state, the switchable grating excites surface plasmon polaritons (SPP) and bulk plasmon polaritons (BPPs) in plasmonic films and hyperbolic metamaterials (HMMs), respectively. The SPP switch has a footprint of 23.1 μm^2 and a MD of up to 40 dB. The BPP switch has a footprint of 13.12 μm^2 and a MD of 29.7 dB. The BPP switch enjoys a broadband MD from 299 to 375 THz. Concurrently, we show that the same switchable grating on plasmonic film and on HMM is a reflection-based optical switch. Finally, we present a novel scheme for non-local control over the spontaneous emission rate and out-coupled power from emitters embedded in HMMs.

Keywords Nano-photonics · Plasmonic switch · Phase change materials · Hyperbolic metamaterials

Introduction

Optical switches are central elements in optical interconnect schemes and optical logic gates [1]. The footprint of the state-of-the-art optical switches, based on MEMS technology, is several hundreds of square micrometres [2]. Plasmonic switches offer a compact alternative to optical switches. The information carriers in plasmonic circuits are surface plasmon polaritons (SPPs); electromagnetic surface waves excited at a metal/dielectric interface. The field associated with SPPs is highly confined and requires a phase matching element, e.g. prisms or diffraction gratings, to couple from free space irradiation. Due to the strong field confinement associated with SPP excitation and their high sensitivity to their surrounding refractive index, highly compact plasmonic switches were demonstrated exploiting the electro-optic [3], magneto-optic effect [4], photo-thermal effect [5], Pauli-blocking in graphene [6], phase-change materials [7] and liquid crystals [8]. The aforementioned methods rely on modifying the dispersion of the SPPs in the plasmonic waveguide by either changing the surrounding dielectric properties, e.g. using an electro-optic material and applying a voltage to induce an index change Δ n [2–4, 7], or through changing the metal's optical properties, e.g. by irradiating it with an ultrafast laser pulse [5]. Therefore, the switching performance becomes intimately dependent on device specific properties such as Δ n, the field intensity in the modulated region, and the quality factor of the modulated mode.

Here, we propose and numerically investigate a plasmonic switching method that can be applied on various plasmonic platforms using a switchable grating. The proposed switchable grating method can be applied to various plasmonic guided mode and plasmonic material. We numerically present a plasmonic switch with a footprint of 23.1 μm^2 and a modulation depth ($MD = 10\mathrm{Log}(I_{ON}/I_{OFF})$) [9], up to 40 dB.

✉ Mohamed ElKabbash
melkabba@ur.rochester.edu

✉ Chunlei Guo
guo@optics.rochester.edu

[1] GPL Photonics Laboratory, State Key Laboratory of Applied Optics, Changchun Institute of Optics, Fine Mechanics and Physics, Chinese Academy of Sciences, Changchun 130033, China

[2] University of Chinese Academy of Science, Beijing 100049, China

[3] The Institute of Optics, University of Rochester, Rochester NY 14627, USA

Footprint is simply a device area given by the product of total device length with device width. As we have used 10 periods of coupling and outcoupling grating with period of 700 nm and separated by 1500 nm, so the total device length is ~ 14.1 μm and lateral width taken as $\sqrt{2\ln(2)}\times$ beam waist size (1.5 μm) ~ 1.64 μm, so the SPP switch footprint is ~ 23.1 μm^2. Moreover, we show that our switch can directly modulate the reflection of an incident beam where photons are information carriers. In addition, we show a novel plasmonic switch based on bulk plasmon polaritons (BPPs)

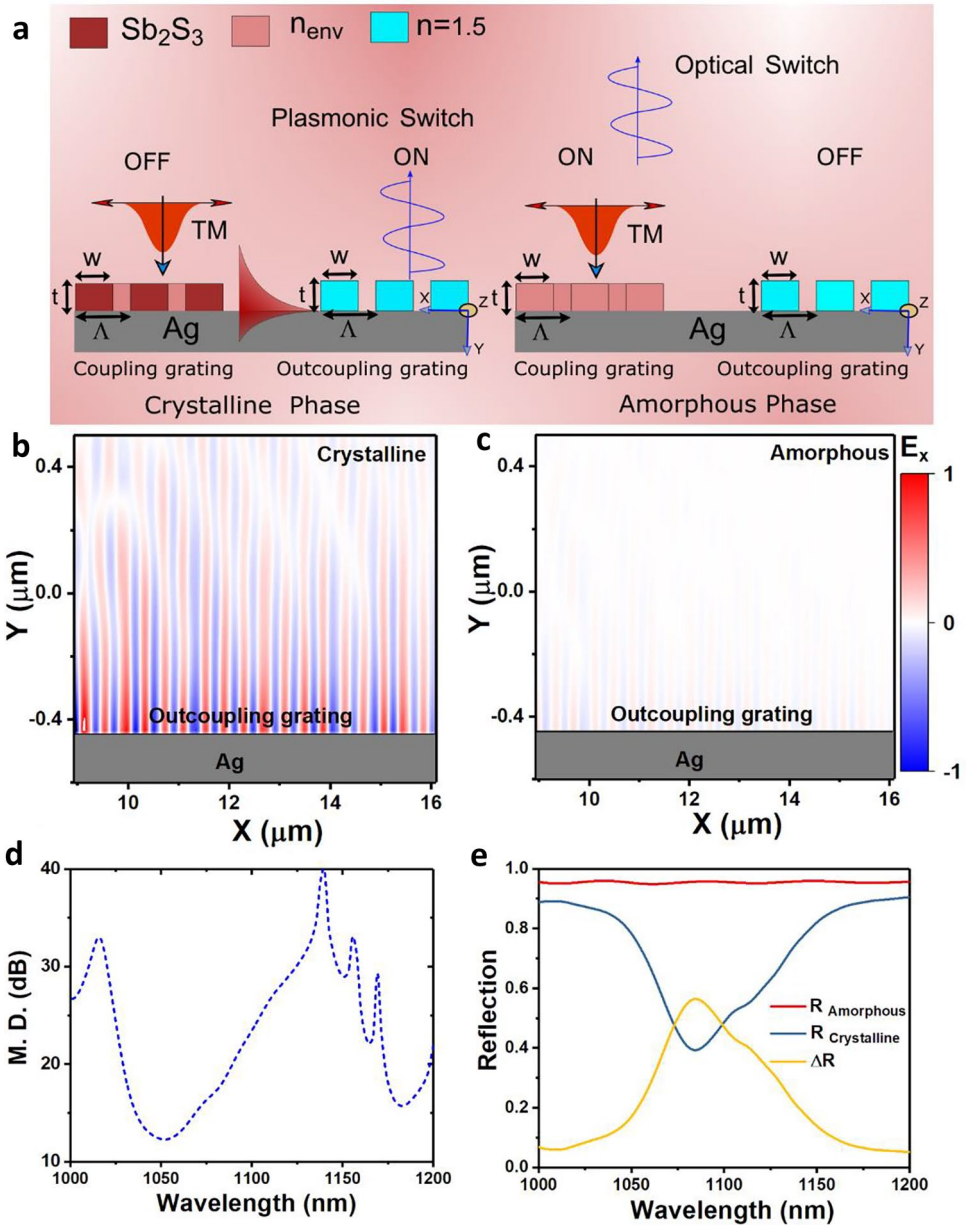

Fig. 1 **a** Schematics of the proposed switchable grating as an SPP switch. When Sb_2S_3 is in its crystalline phase, a substantial index contrast with the dielectric environment exists and the grating is activated. When Sb_2S_3 is in its amorphous state, however, the index contrast reduces significantly, and the grating disappears. The design introduces an optical switch operating based on the reflected light from the coupling grating and a plasmonic switch operating based on light collected from the outcoupling grating. Note that when the photonic switch is in the ON state, the plasmonic switch is in the OFF state and vice versa. FDTD calculation of the electric field E_x component for the switchable grating at 1083 nm captured in the region after coupling grating in the **b** crystalline state and **c** amorphous state. SPP is only excited and then outcoupled to radiation when the grating is in its crystalline state. **d** Modulation depth of the plasmonic switch as a function of wavelength based on light collected from the outcoupling grating. **e** We calculated reflection and reflection difference collected from the coupling grating for photonics switch. Here, Δ R is reflection difference between the crystalline and amorphous phase, $\Delta R = R_{Amorphous} - R_{Crystalline}$. Gaussian light source with TM polarization is used in the simulation to illuminate only the coupling grating. Ten coupling and outcoupling grating periods have been used in the simulation

in hyperbolic metamaterials with a footprint of 14 μm^2 as well as a modulation depth of 29.7 dB. For HMM, the total device length is ~ 8 micron and width ~ 1.64 μm, so the footprint is ~ 13.12 μm^2. Finally, we show that our switchable grating can modulate the density of optical states and the collected emission power of quantum emitters embedded inside HMMs.

Results and Discussion

Figure 1a schematically depicts the proposed plasmonic switch. Our system consists of a coupling grating made of Sb_2S_3, an outcoupling grating and a connecting plasmonic silver (Ag) waveguide. Ag is chosen due for its low optical losses. Grating parameters such as grating width w, thickness t and period Λ have been optimized to excite SPPs in wavelength ranges where Sb_2S_3 has low optical losses. Perfectly matched layer (PML) is chosen as a boundary condition in our 2D simulation for all the boundaries. A TM polarised gaussian light source with 2 μm waist size from 1000 to 1200 nm is used to illuminate the coupling grating for excitation purpose. A metallic substrate can support SPP at the metal–dielectric interface if the phase-matching condition is satisfied. A coupling grating with period Λ can couple the incident radiation at an angle θ to SPPs if: $k_{spp} = k_0 n_{env} \sin\theta + m\frac{2\pi}{\Lambda}$, where k_{spp} is the SPP wavevector, $k_0 = \frac{2\pi}{\lambda_0}$ is the wave vector in free space, and n_{env} is the refractive index of the incidence medium. In our case, the grating consists of a phase change material (Sb_2S_3) embedded in a dielectric with refractive index n_{env}. Sb_2S_3 can switch its phase from crystalline to amorphous optically, using an ultrafast pulsed laser, [9] or thermally, e.g. using ITO or graphene microheaters below the phase change material [10, 11]. The switching rate from the amorphous to crystalline phases of Sb_2S_3 is ~ 10 MHz, which is relatively fast compared to existing optical switches [12, 13]. The grating is designed such that the refractive index of Sb_2S_3 in the amorphous phase is approximately equal to n_{env}. When Sb_2S_3 is in the crystalline phase, the grating is capable of exciting SPPs which travels along the metal–dielectric interface and eventually radiates through the out-coupling grating. When electromagnetic energy is transferred to SPPs, the reflected light from the coupling grating experiences a sudden decrease (reflection anomaly). On the other hand, when Sb_2S_3 is in the amorphous phase, the index contrast with the environment is negligible and the coupling grating effectively disappears. We thus have a plasmonic switch and an

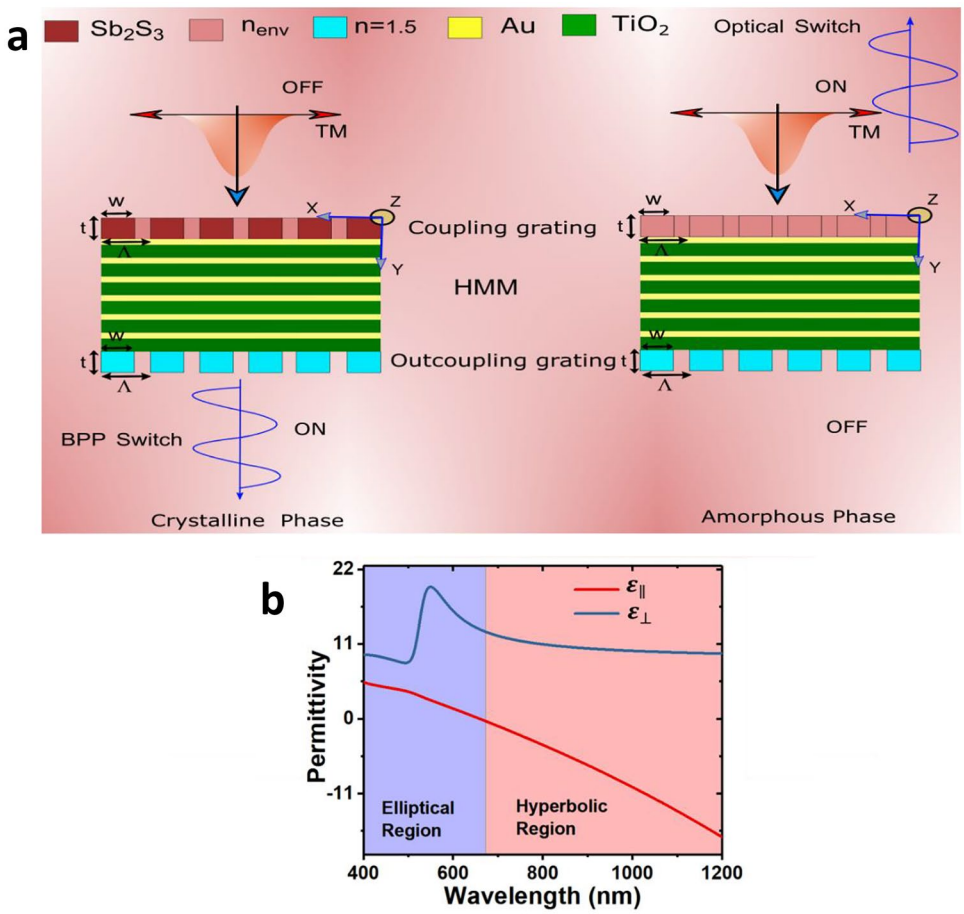

Fig. 2 **a** Schematics of the BPP and optical switch consisting of a switchable grating on an HMM and an outcoupling grating at bottom. The HMM consists of a stack of Au (yellow) and TiO_2 (green) bilayers. When Sb_2S_3 is in its crystalline phase, a substantial index contrast with the dielectric environment exists and the grating is activated. When Sb_2S_3 is in its amorphous state, however, the index contrast reduces significantly, and the grating disappears. The design introduces an optical switch operating based on the reflected light from the coupling grating and a BPP switch operating based on light collected from the outcoupling grating. Note that when the optical switch is in the ON state, the BPP switch is in the OFF state and vice versa. Gaussian light source with TM polarisation focused on coupling grating on the top to excite the BPP. 10 coupling and outcoupling grating periods have been used in the simulation. **b** Effective parallel ($\varepsilon_{\parallel}$) and perpendicular ($\varepsilon_{\perp}$) permittivity of HMM for 5 nm Au and 10 nm TiO_2 unit cell

optical switch. The plasmonic switch is in the ON state, where light detected from the outcoupling grating when the coupling grating is activated, i.e. when Sb_2S_3 is in the crystalline phase. The optical switch is in the ON state when the coupling grating is not activated, i.e. when Sb_2S_3 is in the amorphous phase, and light is reflected back from the coupling grating as it cannot excite SPPs. We numerically investigate our proposed approach using a finite difference time domain (FDTD) commercial software Lumerical®. The coupling grating is made of Sb_2S_3 [13] embedded in a dielectric environment with a refractive index $n_{env} = 2.8$. Possible choices for the dielectric environment are rutile TiO_2 ($n \sim 2.8$) and SiC ($n \sim 2.6$). The 1D grating period, width and thickness are 800 nm, 100 nm, and 500 nm, respectively. The metallic substrate is Ag (permittivity values obtained from chemical rubber company (CRC) press) [14]. The outcoupling grating is made of SiO_2 and placed 1.5 micron away from the coupling grating with a period, width and thickness of 700 nm, 100 nm, and 300 nm, respectively. Normal incident Gaussian source illumination and perfectly matched boundaries were used. Two power monitors were used to detect reflected light from the coupling grating and outcoupled light from the outcoupling grating.

Figure 1b shows the transverse electric field E_x component distribution for Sb_2S_3 in the crystalline phase at resonance wavelength of 1083 nm. The grating successfully excited an SPP with its characteristic exponential decay in the propagation direction and localization at the metal/dielectric interface. On the other hand, when Sb_2S_3 is switched to its amorphous phase, the grating is not activated, i.e. effectively disappears, and no SPP is excited as shown in Fig. 1c. The calculated SPP modulation depth reaches 40 dB

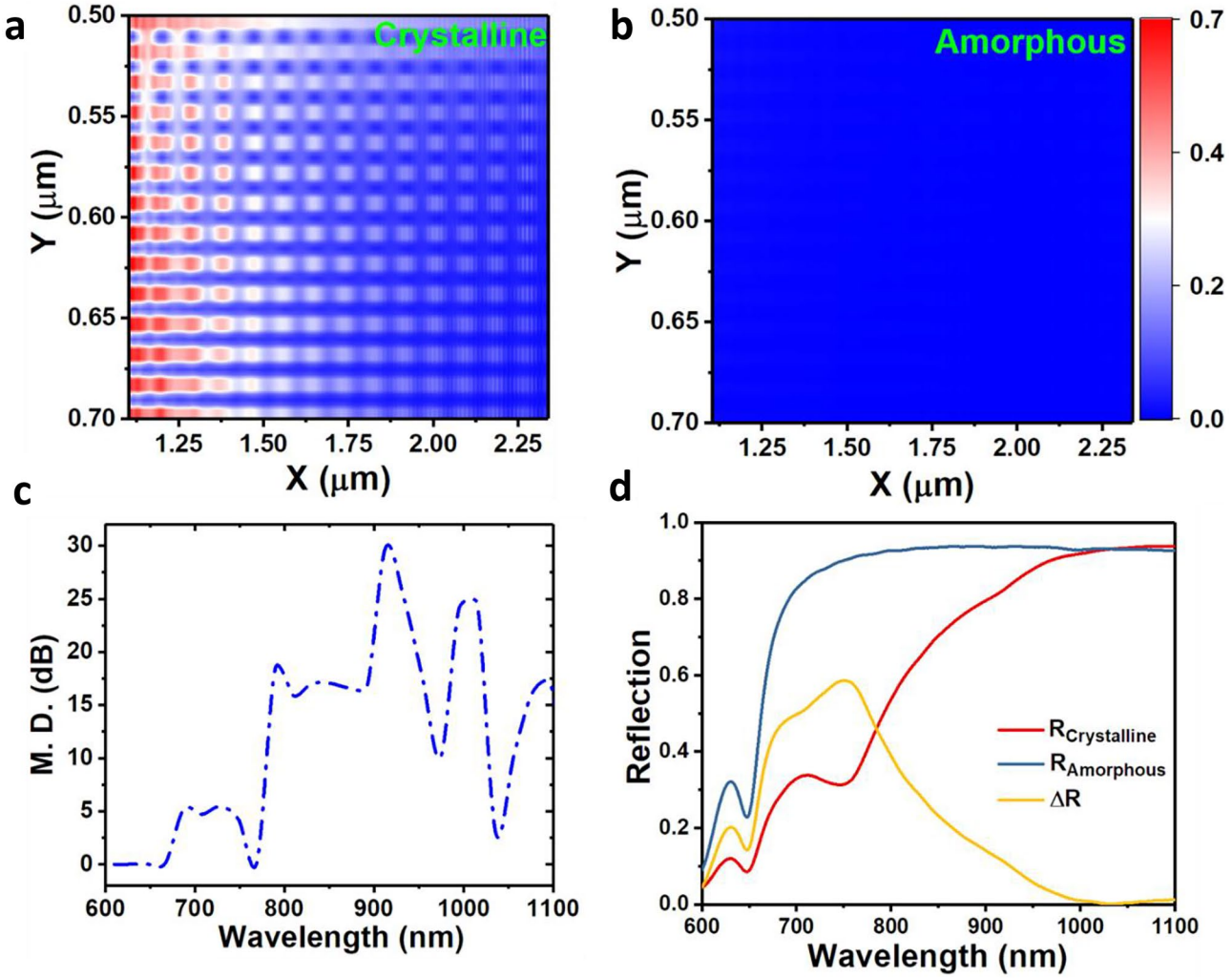

Fig. 3 Simulated field intensity in the HMM when the coupling switchable grating is in its **a** crystalline (ON) state and **b** amorphous (OFF) state. **c** Modulation depth of the BPP plasmonic switch as a function of wavelength based on light collected from the outcoupling grating below. **d** Calculated reflection and reflection difference collected from the coupling grating on top for photonics switch, where $\Delta R = R_{Amorphous} - R_{Crystalline}$

at λ_0 = 1138 nm (see Fig. 1d). The modulation depth is given by 10Log(I_{ON}/I_{OFF}), where I_{ON} and I_{OFF} are the signals detected using the outcoupling grating in case crystalline and amorphous Sb_2S_3 coupling grating, respectively.

In addition to realizing an SPP switch, a direct consequence of our approach is realizing a reflection optical switch. For light incident on the coupling grating, when the grating is switched ON, excitation of SPPs is associated with a dip in reflection within the wavelength range where the grating phase matching condition is satisfied. By monitoring the reflection from the coupling grating, we observe Δ R ~ 0.57 is at λ_0 ~ 1083 nm (see Fig. 1e).

We adopt a similar approach to optically switch the high-k modes of hyperbolic metamaterials (HMMs), i.e. bulk plasmon polaritons (BPP) [15]. HMMs are artificially engineered material with a hyperbolic iso-frequency curve. A common platform for HMMs is metal-dielectric thin film stack where the uniaxial anisotropic permittivity values are such that $\varepsilon_{\parallel} = \varepsilon_x = \varepsilon_z < 0$ and $\varepsilon_{\perp} = \varepsilon_y > 0$. The positive perpendicular permittivity is due to the ability of these HMMs to excite bulk modes that consist of evanescently coupled SPPs, i.e. BPPs.

Because the local density of optical states (LDOS) are related to the volume enclosed by the iso-frequency surface [16], HMMs enjoy high LDOS which leads to various effects enhanced Purcell factors or quantum emitters [16], perfect light absorption [17, 18] and long-range dipole–dipole interactions [19]. HMM-based optical switches relied on switching the topological transition frequency using an HMM with an active element, e.g. a phase change material or graphene [20, 21]. In these works, however, BPP was not the information carrier, rather the reflected photons from the HMM. By using a switchable coupling grating and placing an out-coupling grating at the bottom of the HMM [22], we can create an optical switch based on BPPs (Fig. 2). The coupling grating consists of

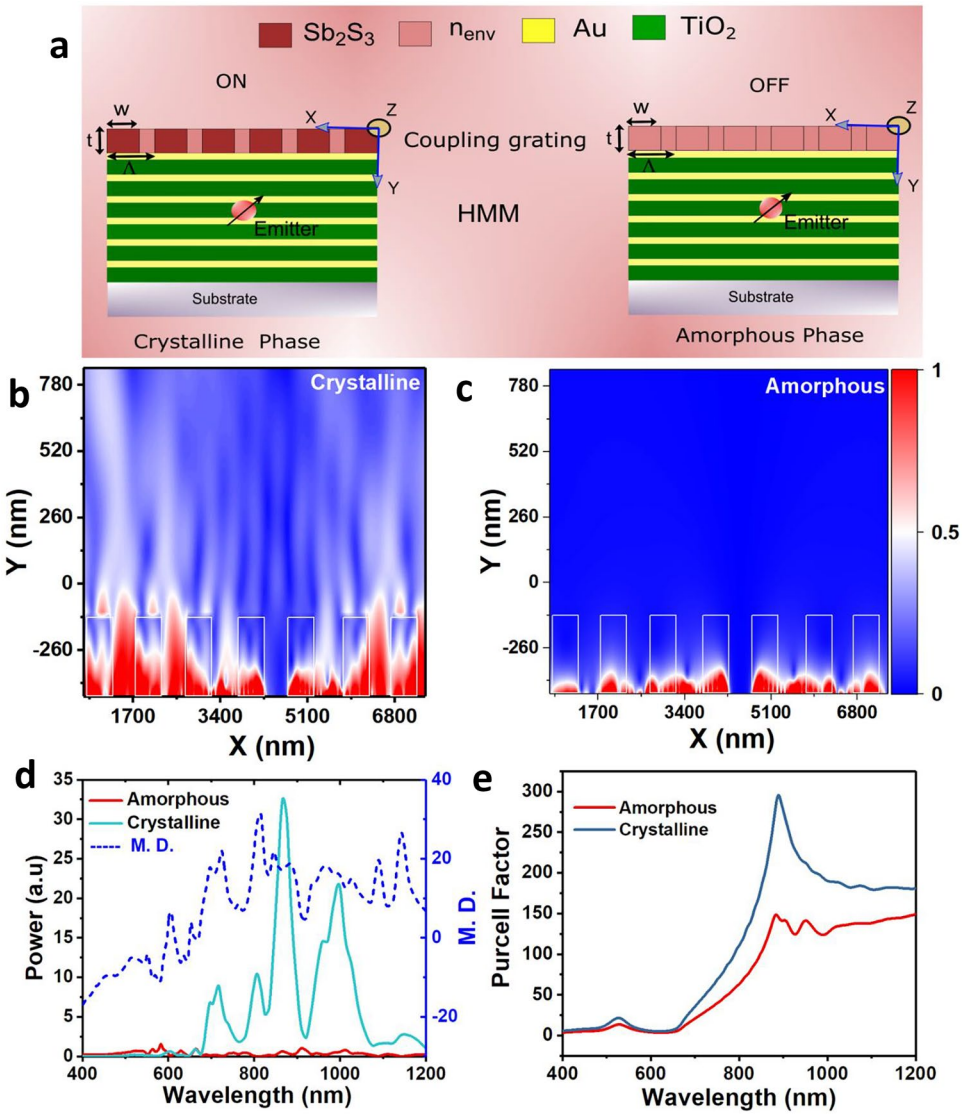

Fig. 4 **a** Schematics of an emitter (vertical dipole) embedded in an HMM with a switchable grating to non-locally control the spontaneous emission rate of the emitter. When Sb_2S_3 is in its crystalline phase, a substantial index contrast with the dielectric environment exists and the grating is activated. When Sb_2S_3 is in its amorphous state, however, the index contrast reduces significantly, and the grating disappears. The thickness of Au and TiO_2 are 5 nm and 10 nm. The grating parameters are :w= 500 nm, t = 310 nm and 1000 nm, nenv= 2.8.Electric field profile in **b** crystalline phase and **c** amorphous phase, coupling grating is shown with white rectangles. **d** Calculated far field power radiated in the crystalline (ON) and amorphous (OFF) phase and modulation depth. **e** The calculated Purcell factor in the crystalline and amorphous phase

Sb_2S_3 embedded in a dielectric environment with a refractive index $n_{env} = 2.8$. The grating parameters such as grating width w, grating thickness t and grating period Λ are optimized to have resonance in the region where Sb_2S_3 losses are negligible. The optimized grating period, width and thickness are 1000 nm, 500 nm and 310 nm. The outcoupling grating refractive index is 1.5 and has the same dimensions as the coupling grating.

Our HMM consists of 24 bilayers of Au (5 nm) and TiO_2 (10 nm) thin films. The perpendicular and parallel permittivity of the system are given by $\varepsilon_{\parallel} = f_m\varepsilon_m + f_d\varepsilon_d$ and $\varepsilon_{\perp} = \frac{\varepsilon_m\varepsilon_d}{f_m\varepsilon_m + f_d\varepsilon_d}$, respectively, and calculated in Fig. 2b [15]. The topological transition occurs when $\varepsilon_{\perp} < 0$ at ~ 600 nm as shown in Fig. 2b. Figure 3a shows the calculated electric field intensity for the HMM. When the grating is in the crystalline phase, BPPs are excited inside the HMM. Conversely, when the grating is in the amorphous phase, BPPs are not excited (see Fig. 3b). Nearly 29.7 dB modulation depth of BPPs at ~ 900 nm (see Fig. 3c) is obtained. Moreover, high MD is obtained over a wide range of wavelengths (800–1000 nm) with an average MD of 18 dB. However, the ultrahigh MD comes at the cost of increasing the insertion loss. The insertion loss of the BPP switch is −33 dB while for SPP switch is less than 10 dB. Moreover, due to the high LDOS of HMMs, the reflection drop associated with switching the grating ON and exciting BPPs is stronger than the case of SPPs. Consequently, we obtain a Δ R of ~ 0.55 at 750 nm as shown in Fig. 3d. The calculated effective index of fundamental mode at 750 nm is $2.7 + i0.012$ using FDE solver in Lumerical mode solution. The effective index calculation suggests the grating period in order to excite the BPP mode [23].

The high LDOS of HMMs can accelerate the spontaneous emission rate of quantum emitters coupled via their near fields to the HMMs high-k modes [15]. Emitters located inside the HMM excite BPPs through their near field. Therefore, the emission remains mostly trapped and eventually dissipates because of the momentum mismatch between BPPs and free space radiation. Using a grating is essential to out-couple the emission of emitters embedded inside HMMs [24]. We show here that our switchable grating can be used to control the coupling of quantum emitters to radiation and to nonlocally control the emitter's spontaneous emission rate. Figure 4a schematically shows our calculation setup where a dipole is placed within the HMM. When the grating is switched ON in the crystalline phase, the emission out-couples from the HMM, i.e. the system behaves as a switch for emission collected from quantum emitters as shown in electric field profile of the emitted radiation (Fig. 4b). However, in the amorphous phase, where the grating effectively disappears, the emission trapped inside the HMM (Fig. 4c). Figure 4d shows a high modulation depth of up to 31 dB when grating is in crystalline phase i.e. ON state. We note that the HMM increases the Purcell factor of the emitter due to the HMM high local density of optical states (LDOS). Because the LDOS depends on the number of propagating and evanescent states available to the emitter to radiate into, when the grating is ON, the Purcell factor significantly increases by 100% (from 150 to 300 at 840 nm). Moreover, only when the grating is ON, i.e. Sb_2S_3 in the crystalline phase, the emission is out coupled and detected outside the HMM as shown in Fig. 4e.

Conclusion

In conclusion, we proposed a method for a plasmonic switch that controls the excitation of SPPs in plasmonic films and BPPs in HMMs. The SPP switch enjoys a footprint of 23.1 μm^2, 40 dB MD and less than 10 dB insertion loss, while the BPP switch has a footprint of 13.1 μm^2, 29.7 dB MD, and − 33 dB insertion loss. The small footprint of the proposed plasmonic switches makes them as building blocks of high space-–bandwidth spatial light modulators [25] Finally, we showed that our approach can non-locally control the LDOS and outcoupling of spontaneous emission from quantum emitters coupled to HMMs high-k modes with an MD reaching 31 dB. The plasmonic switch offers an attractive option for ultracompact and high modulation depth applications. The proposed concept can be extended to tunable metasurfaces [26], e.g. for tunable beam deflection, guided mode resonances and bound state in the continuum modes [27].

We finally note that optical losses are the biggest problem facing all plasmonic devices and switches. Unless new plasmonic materials appear that exhibit low optical losses, it will remain a niche alternative where significantly decreasing the device footprint is desirable as shown in our work. For instance, an important metric for spatial light modulators, which can consist of an array of optical switches, is the space-bandwidth product which is represented by the product of the pixel footprint of individual optical switches in an SLM and the largest spatial size over which these pixels can extend. The space-bandwidth product corresponds to the total number of parallel channels of data that the SLM can encode and hence is an important performance metric [25]. Operating at longer wavelengths using doped semiconductors[28], adding gain material [29, 30], discovering of low loss plasmonic materials [27] or exciting other types of lower loss plasmonic modes such as long-range surface plasmons [31], are all possible ways to reduce losses.

Acknowledgements S. K. C. acknowledges his sponsorship by "CAS-TWAS Presidential Fellowship for international doctorate students."

Author Contribution Conceptualization, M. E.; methodology, M. E. and S. K. C.; software, S. K. C. and M. E.; validation, S.K.C., M.E. and C.G.; formal analysis, S. K. C.; investigation, S. K. C. and M. E.; writing original draft preparation, M. E. and S. K. C.; writing review and editing, S.K.C., M.E. and C. G.; supervision, M.E., C. G.; project administration, C. G.

Funding National Natural Science Foundation (11674178); Jilin Provincial Science and Technology Development Project (20180414019GH); and Bill & Melinda Gates Foundation (INV-009181).

Data Availability The data that support the findings of this study are available from the corresponding author upon reasonable request. The data for this research work is available upon request.

Code Availability The code that supports the findings of this study are available upon reasonable request.

Declarations

Ethical Statement Hereby, I Sandeep Chamoli, consciously assures that for the manuscript titled "Switchable Gratings for Ultracompact and Ultrahigh Modulation Depth Plasmonic Switches," the following is fulfilled:

1. This material is the authors' own original work, which has not been previously published elsewhere.
2. The paper is not currently being considered for publication elsewhere.
3. The paper reflects the authors' own research and analysis in a truthful and complete manner.
4. The paper properly credits the meaningful contributions of co-authors and co-researchers.
5. The results are appropriately placed in the context of prior and existing research.
6. All sources used are properly disclosed (correct citation). Literally copying of text must be indicated as such by using quotation marks and giving proper reference.
7. All authors have been personally and actively involved in substantial work leading to the paper, and will take public responsibility for its content.

The violation of the Ethical Statement rules may result in severe consequences.

I agree with the above statements and declare that this submission follows the policies of Plasmonics Journal as outlined in the Guide for Authors and in the Ethical Statement.

Consent to Participate Informed consent was obtained from all individual participants included in the study.

Consent for Publication There are no case studies involve in the current work. Therefore, this declaration is not applicable in our case.

Conflict of Interest The authors declare no competing interests.

References

1. Zhang X, Yang J (2019) Ultrafast plasmonic optical switching structures and devices. Front Phys 7:190
2. Emboras A, Hoessbacher C, Haffner C, Heni W, Koch U, Ma P, Fedoryshyn Y, Niegemann J, Hafner C, Leuthold J (2014) Electrically controlled plasmonic switches and modulators. IEEE J Sel Top Quantum Electron 21:276–283
3. Cai W, White JS, Brongersma ML (2009) Compact, high-speed and power-efficient electrooptic plasmonic modulators. Nano Lett 9:4403–4411
4. Haddadpour A, Nezhad VF, Yu Z, Veronis G (2016) Highly compact magneto-optical switches for metal-dielectric-metal plasmonic waveguides. Opt Lett 41:4340–4343
5. MacDonald KF, Sámson ZL, Stockman MI, Zheludev NI (2009) Ultrafast active plasmonics. Nat Photonics 3:55–58
6. Ono M, Hata M, Tsunekawa M, Nozaki K, Sumikura H, Chiba H, Notomi M (2020) Ultrafast and energy-efficient all-optical switching with graphene-loaded deep-subwavelength plasmonic waveguides. Nat Photonics 14:37–43
7. Lee S-Y (2017) Design of a plasmonic switch using ultrathin Chalcogenide phase-change material. Curr Opt Photonics 1:239–246
8. Liu YJ, Zheng YB, Shi J, Huang H, Walker TR, Huang TJ (2009) "Optically switchable gratings based on azo-dye-doped, polymer-dispersed liquid crystals," Opt. Lett. 34, 2351–2353
9. Reed GT, Mashanovich G, Gardes FY, Thomson D (2010) Silicon optical modulators. Nat Photonics 4:518–526
10. Ríos C, Zhang Y, Deckoff-Jones S, Li H, Chou JB, Wang H, Shalaginov M, Roberts C, Gonçalves C, Liberman V, Gu T, Kong J, Richardson K, Hu J (2019) "Reversible switching of optical phase change materials using graphene microheaters," Opt. InfoBase Conf. Pap. Part F129-, 10–11
11. Au Y-Y, Bhaskaran H, Wright CD (2017) Phase-change devices for simultaneous optical-electrical applications. Sci Rep 7(1):9688
12. Chamoli SK, Verma G, Singh S, Guo C (2021) Phase change material-based nano-cavity as an efficient optical modulator. Nanotechnol 32:095207
13. Delaney M, Zeimpekis I, Lawson D, Hewak DW, Muskens OL (2020) A new family of ultralow loss reversible phase-change materials for photonic integrated circuits: Sb_2S_3 and Sb_2Se_3. Adv Funct Mater 2002447.
14. CRC handbook of chemistry and physics (1977) Cleveland. CRC Press, Ohio
15. Chamoli SK, ElKabbash M, Zhang J, Guo C (2020) Dynamic control of spontaneous emission rate using tunable hyperbolic metamaterials. Opt Lett 45:1671–1674
16. Krishnamoorthy HN, Jacob Z, Narimanov E, Kretzschmar I, Menon VM (2012) Topological transitions in metamaterials. Science 336:205–209
17. Guclu C, Campione S, Capolino F (2012) Hyperbolic metamaterial as super absorber for scattered fields generated at its surface. Phys Rev B 86:205130
18. Narimanov EE, Li H, Barnakov YA, Tumkur T, Noginov M (2013) Reduced reflection from roughened hyperbolic metamaterial. Opt Express 21:14956–14961
19. Newman WD, Cortes CL, Afshar A, Cadien K, Meldrum A, Fedosejevs R, Jacob Z (2018) Observation of long-range dipole-dipole interactions in hyperbolic metamaterials. Sci Adv 4:eaar5278
20. Liang W, Li Z, Wang Y, Chen W, Li Z (2019) All-angle optical switch based on the zero-reflection effect of graphene–dielectric hyperbolic metamaterials. Photonics Res 7:318–324
21. Shoaei M, Moravvej-Farshi MK, Yousefi L (2015) All-optical switching of nonlinear hyperbolic metamaterials in visible and near-infrared regions. JOSA B 32:2358–2365
22. Xu T, Lezec HJ (2014) Visible-frequency asymmetric transmission devices incorporating a hyperbolic metamaterial. Nat Commun 5:4141
23. Sreekanth K, De Luca A, Strangi G (2013) Experimental demonstration of surface and bulk plasmon polaritons in hypergratings. Sci Rep 3:3291

24. Lu D, Kan J, Fullerton E et al (2014) Enhancing spontaneous emission rates of molecules using nanopatterned multilayer hyperbolic metamaterials. Nat Nanotechnol 9:48–53
25. Neff JA, Athale RA, Lee SH (1990) Two-dimensional spatial light modulators: a tutorial. Proc IEEE 78:826–855
26. Jin C, Zhang J, Guo C (2019) Metasurface integrated with double-helix point spread function and metalens for three-dimensional imaging. Nanophotonics 8:451–458
27. Hsu C, Zhen B, Stone A et al (2016) Bound states in the continuum. Nat Rev Mater 1:16048
28. Khurgin JB (2015) How to deal with the loss in plasmonics and metamaterials. Nat Nanotechnol 10:2–6
29. El Kabbash M, Rahimi Rashed A, Sreekanth KV, De Luca A, Infusino M, Strangi G (2016) Plasmon-exciton resonant energy transfer: across scales hybrid systems. J Nanomater 2016
30. ElKabbash M, Rashed AR, Kucukoz B, Nguyen Q, Karatay A, Yaglioglu G, Ozbay E, Caglayan H, Strangi G (2017) Ultrafast transient optical loss dynamics in exciton–plasmon nano-assemblies. Nanoscale 9:6558–6566
31. Berini P (2009) Long-range surface plasmon polaritons. Adv Opt Photonics 1:484–588